Cryogenic Land Surface Process Detection in Siberian High Latitude Mountain Permafrost Landscape by Time Series Landsat Thermal Imagery

Sébastien Gadal, Moisei Zakharov

IGARSS 2023 - 2023 IEEE International Geoscience and Remote Sensing Symposium | 979-8-3503-2010-7/23/$31.00 ©2023 IEEE | DOI: 10.1109/IGARSS52108.2023.10282807

CRYOGENIC LAND SURFACE PROCESS DETECTION IN SIBERIAN HIGH LATITUDE MOUNTAIN PERMAFROST LANDSCAPE BY TIME SERIES LANDSAT THERMAL IMAGERY

Sébastien Gadal, Moisei Zakharov

Aix Marseille Univ, Université Côte d'Azur, Avignon Université, CNRS, ESPACE, UMR 7300, 84000 Avignon, France

ABSTRACT

In recent years, the accumulation of cloud-free remote sensing thermal infrared data for high-latitude permafrost regions makes it possible to use them to identify active cryogenic land surface processes (ACP) spurred by climate change and human activities. ACP is an extremely important indicator of excitations in the energy cycle of permafrost landscapes and changes in the carbon budget. In this paper, we test the time series of land surface temperature (LST) extracted from Landsat 8 OLI/TIRS datasets using a split window algorithm (SWA) to identify ACP for the study area in the mountains of Northeastern Siberia. We identified active cryogenic processes from thermal anomalies detected using standard deviation thresholds on 5 datasets for selected dates. Our results show that multi-year verified high-resolution LST data for the second half of the summer period can be applicable for identifying an area with active cryogenic processes in valley and disturbed permafrost landscapes, provided they can indicate local effects of processes associated with drainage degradation and vegetation change.

Index Terms— land surface temperature, split-window algorithm, thermal anomaly, land surface cryogenic process, Landsat

1. INTRODUCTION

The permafrost landscapes of the Arctic, including in mountainous regions, are undergoing significant changes driven by climate change, which provokes permafrost degradation and shifts in the boundaries of boreal forests and alpine tundra [1]. For mountainous permafrost regions, wet tundra, burned areas and wetlands in river valleys concentrate dynamic permafrost processes, particularly ACP. ACP are associated with the seasonal and long-term dynamics of freezing and thawing of permafrost and vein ice that form the microrelief, thereby disturbing the energy and water cycles in landscapes [3]. By active we mean developing processes, beyond the functioning of permafrost landscapes. For permafrost with a high ice content, the main ACP are: thermokarst, frost cracking, solifluction, and frost heaving. These processes are the principal mechanism of the climate-driven evolution of permafrost landscapes. River valleys and bare soils in mountainous regions are the most valuable landscapes for nature management and transport infrastructure, the detection of ACP as areas containing critical thermal resistance classes can contribute to risk planning for land use and vulnerability assessment for the infrastructure. Furthermore, the studies indicate that the areas with cryogenic disturbance make the largest contribution to carbon emissions from permafrost [2].

The most vulnerable to the development of cryogenic processes are poorly drained areas with ice wedges in the permafrost, the so-called ice-rich permafrost landscapes [3]. We put forward a hypothesis about the possible role of active cryogenic processes, in which stress conditions in the hydrothermal regime of landscapes cause abnormal thermal infrared signals in satellite sensors. From this follow the research questions to which the paper is devoted: (1) whether the use of multitemporal thermal imaging makes it possible to detect well the development of AKP and (2) which ACP and types of mountain permafrost landscapes are limited using this detection method.

2. MATERIALS AND METHODS

2.1. Study area

We tested our hypothesis in study area with 60x100 km size located on the eastern slope of the Verkhoyansk Mountains in Northeast Siberia. In the previous studies we conducted a detailed mapping of permafrost landscape types for this region [4]. 22 landscape types of tundra, boreal forests, and glacial valleys are distributed within the study area, which, in fact, represents the full gradient of arctic mountain landscapes. The climate of the region is characterized as extreme continental with short warm summers and long very cold winters. This region in previous studies does not suggest the presence of ice-rich permafrost [3], but wetlands and meadows in river valleys are covered by thermokarst,

heaving and frost cracking with the development of a polygonal microrelief, that we noted in our in-situ field observations.

2.2. Datasets

Landsat 8 data with two thermal bands along with visible/nearest infrared bands were used for LST retrieval. To apply LST, we conducted a minimum-noise filter to select the data, which significantly reduces the temporal range of the dataset. From 12 cloudless Landsat 8 OLI/TIRS over the summer period (June-August), five datasets were selected after clipping and evaluating for smoke from forest fires, passing rainfall by weather data, see Table 1.

Table 1. Parameters of Landsat OLI/TIRS 8 datasets

Date	Landsat 8 OLI/TIRS		MODIS LST	Weather station T_{air} °C
	Sun elevation (°)	Scene time (GMT +9)	Scene time (GMT +9)	
29/07/2013	37.9	11:59	15:36	21,2
9/08/2017	37.3	11:57	14:48	19,1
28/08/2018	31.3	11:57	14:12	16,4
1/08/2020	39.4	11:57	14:48	19,8
4/08/2021	38.7	11:58	14:24	19,8

All Landsat surveys were performed at noon with a minimum time difference. To test the use of LST daytime MODIS performed mostly in the afternoon. According to the meteorological station at mid-day, the weather in the study area was clear, there was no rain during the week before the shooting.

2.2. Time series Land surface temperature

We have chosen the split window algorithm for LST retrieval, which corrects atmospheric effects based on the differential absorption of the two thermal bands [5]. Thus, this LST retrieval technique uses the advantages of Landsat 8, which has TIRS bands in the 10-12.5 μm window. SWA is effective in detecting surface thermal variability over time and space ranges [6],[7]. Two approaches to SWA as formulated by Qin et al.[8] and Sobrino et al.[9] can be distinguished in the literature, which are derived from the first order linearization of the Taylor series in the radiative transfer equation and basically have the following equation with Landsat 8 OLI/TIRS:

$$LST = a_0 + a_1 BT_{10} - a_2 BT_{11}$$

where BT_{10} and BT_{11} are the brightness temperatures of the 10 and 11 TIR bands, respectively, and a_0, a_1, and a_2 are the coefficients determined by the atmospheric transmittance and the land surface emissivity. We use a modified Qin approach, for which the calculation of these variables is described in Rosenstein et al. [10]. For Landsat 8 TIRS the effect of the zenith angles is not considered [11]. The atmospheric transmittance has been simulated using the MODTRAN 6.0 for the standard atmospheric profiles of sub-arctic summer. The emissivity of the earth's surface was estimated by the NDVI threshold method, extracting the proportions of soil (sparse vegetation and lichen tundra) (NDVI < 0.2) and vegetation (forest and high biomass valley landscapes) (NDVI > 0.45). The methodological workflow of the LST extraction in our case is shown in Figure 1.

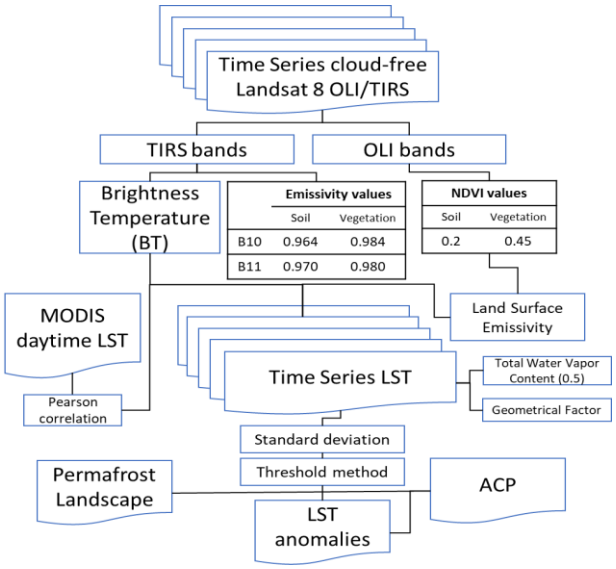

Figure 1. Methodological workflow for retrieving LST by Split-Window algorithm

2.3. LST validation

The obtained LST values were verified by comparison with MODIS daytime LST at 1 km spatial resolution and air temperature data from meteorological stations operating in the study area. Due to extensive testing, MODIS LST products are considered as high quality and often used for validation [12]. Validation with MODIS LST showed Pearson correlation coefficients of 0.76-0.81, the difference between the mean values of the two data sets yielded a statistically significant difference in mean values at 2.1 ◦C, which is associated with spatial differences while maintaining trends. In addition, the extreme continental nature of the climate means that there are large variations in temperature, meaning that the time difference can play a significant role in August, as the effect of polar days is reversed.

Comparing LST with air temperature data from meteorological stations operating in Batagai-Alyta, we used mean LST value in a 3x3 window with geolocation pixel of the weather station. We observe air temperature values lower than those of LST with trends and differences well observed.

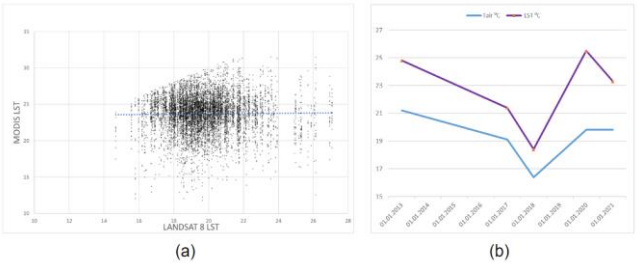

Figure 1. (a) Linear regression of LST MODIS with LST obtained by Landsat 8 in the study area (b) Comparison of LST obtained by Landsat 8 with air temperature from a weather station

2.4. ACP recognition by LST standard deviation

LST is known to be influenced by biophysical surface parameters, including energy and moisture fluxes [13]. Permafrost thawing and changes in seasonal vegetation dynamics as well as forest fires are reflected in thermal anomalies in the LST time series. We propose to use the measurement of the standard deviation for the thermal anomalies (Fig. 2) in the time series of LST values.

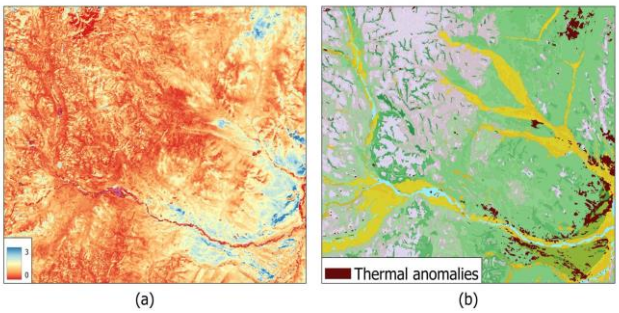

Figure 2. ACP detection using time series LST by Landsat 8: (a) standard deviation of the time series LST; (b) thermal anomalies distribution in the study area.

A standard deviation with an excess of more than 2.4σ, which is a threshold, was defined as a probable anomaly relative to normal surface heat radiation. After processing the preliminary data and checking for errors, we found that the anomalies were most typical for open areas with excess moisture and young burnt areas, which is associated with forest fires in the area in 2018.

4. RESULTS

High standard deviation values reflect strong variations in LST values, which are associated with variations in moisture content, changes in vegetation cover due to forest fires and anthropogenic impacts along roads (Fig. 2, a). Thermal anomalies correspond to potential changes in the hydrothermal regime of permafrost landscapes observed in these parts of the landscapes during frost thaw peaking in August (Fig. 2, b). In addition, the area of anomalies covers the burned areas, where post-wildfire transformation causes changes in the thermal regime of the landscape and generation of ACP [9], [10].

Most of the detected ACP areas are associated with three types of landscapes: mountain sparse moss lichen forests in gentle fluvioglacial slopes, boggy meadows with low shrubs in mid-altitude terraces, and larch low shrubs forests with boggy meadows in alluvial low terraces (Fig. 3). Anomalies in the LST time series for these types of landscapes, are associated with the swelling influence of watercourses (taliks) in the low and middle-altitude parts of the valleys of large mountain rivers.

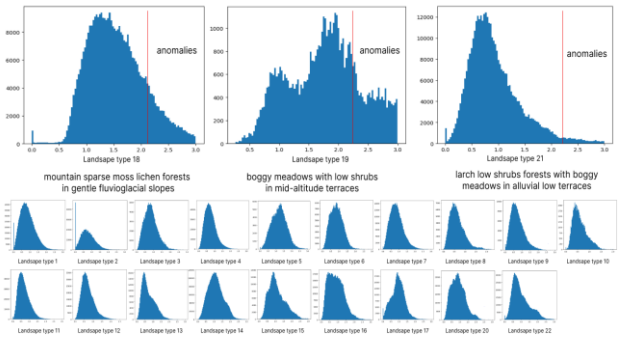

Figure 3. Histograms of standard deviation LST values by types of permafrost landscapes with detection of thermal anomalies

The fraction of ACP area for forest types of landscapes is 0.8%, for tundra, 0.03% and for river valleys 1.6%. In these landscapes on alluvial sands and turf with thicknesses up to 0.6-1.3 m, frost heaving is the most widely distributed, reaching up to 6-22 pcs/100 sq. m in treeless areas.

5. DISCUSSION

The multiyear dynamics of the LST, as suitable data are accumulated, allow the mapping of areas with disturbed hydrothermal regime, which is most clearly visible in the second half of the summer season, when the effect of seasonally thawing permafrost is most significant.

The use of multi-year, high-resolution thermal infrared imagery data allows their ACP to be identified for non-forested landscapes and areas of disturbed cover. In existing permafrost maps, the area is defined as a non-forest-rich permafrost zone. Therefore, the use of the LST time series makes it possible to define new areas of local distribution of talik and ice-rich permafrost, as they are the most responsive to climate change. The distribution of ACP detected by LST can indicate the presence of ice veins in local areas. In the future, the method may serve as an extension of the methodology for the detection of hazardous permafrost areas.

Due to the large LST differences between forests, burnt areas and wetlands that we observed, a significant permafrost warming effect from cryogenic processes is expected. The thermal anomalies identified are related to the effect of surface warming during disturbance of natural cover, because

of forest fires, which alters the surface energy balance and the water cycle. Early studies show that surface cryogenic processes increase in poorly drained bare areas, responding to climatic changes

Considering the uncertainties of satellite LST, the results of the present work should be assessed with caution. It is well known that LST values can be affected by several factors, such as rainfall, fire and evapotranspiration can cause spatio-temporal anomalies in the LST [14]. Although we have tried to minimize this effect, the more we have greatly reduced the temporal range. Therefore, we argue that the use of sufficiently long time series of LST retrievals can distinguish stable thermal patterns of cryogenic processes.

6. CONCLUSION

In this short paper, we describe a technique for detecting cryogenic processes in mountain permafrost landscapes from LST time series from Landsat 8 TIRS data, using a split window algorithm. The results showed that using thermal infrared imagery over large areas to detect cryogenic processes by LST time series. As noted in many studies, satellite thermal imagery and LST derived images are heavily contaminated by cloud cover, atmospheric effects, and weather dynamics. Consistent detection of permafrost landscape features using ACP requires a wider temporal range of satisfactory images. The ACPs we have identified contain noise associated with denuded mountain slopes. Promising high-resolution thermal infrared imaging missions, such as the French-Indian TRISHNA (Thermal infraRed Imaging Satellite for High-resolution Natural Resource Assessment) mission [15], will allow future advances in cryogenic process mapping, which will be aimed at improving the methodology in future studies.

7. ACKNOWLEDGMENTS

This research was supported by the CNES TOSCA TRISHNA “Thermal infraRed ImagingSatellite for High-resolution Natural resource Assessment”.

8. REFERENCES

[1] Pearson, R., Phillips, S., Loranty, M. et al. Shifts in Arctic vegetation and associated feedbacks under climate change. *Nature Clim Change* 3, 673–677, 2013

[2] Aalto, J., Niittynen, P., Riihimäki, H. et al. Cryogenic land surface processes shape vegetation biomass patterns in northern European tundra. *Commun Earth Environ* 2, 222, 2021

[3] Shestakova, A.A.; Fedorov, A.N.; Torgovkin, Y.I.; Konstantinov, P.Y.; Vasyliev, N.F.; Kalinicheva, S.V.; Samsonova, V.V.; Hiyama, T.; Iijima, Y.; Park, H.; et al. Mapping the Main Characteristics of Permafrost on the Basis of a Permafrost-Landscape Map of Yakutia Using GIS. *Land*, 10, 462, 2021

[4] Zakharov, M.; Gadal, S.; Kamičaitytė, J.; Cherosov, M.; Troeva, E. Distribution and Structure Analysis of Mountain Permafrost Landscape in Orulgan Ridge (Northeast Siberia) Using Google Earth Engine. *Land*, 11, 1187. 2022

[5] Rongali, G., Keshari, A.K., Gosain, A.K. et al. Split-Window Algorithm for Retrieval of Land Surface Temperature Using Landsat 8 Thermal Infrared Data. *J geovis spat anal* 2, 14 (2018).

[6] Yan, Y., Mao, K., Shi, J. et al. Driving forces of land surface temperature anomalous changes in North America in 2002–2018. Sci Rep 10, 6931 (2020).

[7] Batbaatar, J., Gillespie, A., Sletten, R., et al. Toward the Detection of Permafrost Using Land-Surface Temperature Mapping. *Remote Sensing* 2, 12, 695, 2020

[8] Qin, Z., Dall'Olmo, G., Karnieli, A., and Berliner, P. (2001), Derivation of split window algorithm and its sensitivity analysis for retrieving land surface temperature from NOAA-advanced very high-resolution radiometer data, *J. Geophys. Res*., 106(D19), 22655– 22670

[9] Sobrino, J.A.; Li, Z.; Stoll, M. P.; & Becker, F. Improvements in the split-window technique for land surface temperature determination. *IEEE Transactions on Geoscience and Remote Sensin*g, vol. 32, no. 2, pp. 243-253, 1994

[10] Rozenstein, O.; Qin, Z.; Derimian, Y.; Karnieli, A. Derivation of Land Surface Temperature for Landsat-8 TIRS Using a Split Window Algorithm. *Sensors*, 14, 5768-5780. 2014

[11] Yu, X.; Guo X. Wu, Z. Land surface temperature retrieval from Landsat 8 TIRS—Comparison between radiative transfer equation-based method split window algorithm and single channel method, *Remote Sensing*, vol. 6, pp. 9829-9852, 2014.

[12] Gemitzi, A., Dalampakis, P., & Falalakis, G. Detecting geothermal anomalies using Landsat 8 thermal infrared remotely sensed data. *Int. J. Appl. Earth Obs. and Geoinf*. 96, 102283, 2021

[13] Liu, S. et al., Detection of Geothermal Anomaly Areas With Spatio-Temporal Analysis Using Multitemporal Remote Sensing Data," *IEEE Journal of Selected Topics in Applied Earth Observations and Remote Sensing*, vol. 14, pp. 4866-4878, 2021

[14] Du, C.; Ren, H.; Qin Q.; Meng, J.; Li, L. Split-Window algorithm for estimating land surface temperature from Landsat 8 TIRS data. 2014 *IEEE Geoscience and Remote Sensing Symposium*, Quebec City, QC, Canada, 2014, pp. 3578-3581

[15] Lagouarde J.-P. et al., The Indian-French Trishna Mission: Earth Observation in the Thermal Infrared with High Spatio-Temporal Resolution, *IGARSS 2018 - 2018 IEEE International Geoscience and Remote Sensing Symposium*, Valencia, Spain, pp. 4078-4081. 2018